Inorganica Chimica Acta 453 (2016) 488–493

Contents lists available at ScienceDirect

Inorganica Chimica Acta

journal homepage: www.elsevier.com/locate/ica

Research paper

Two new complexes constructed by semirigid carboxylic acid ligand: Synthesis, crystal structures, absorption of organic dye and photoluminescence properties

Ya-Jun Wu, Dong-Cheng Hu, Xiao-Qiang Yao, Yun-Xia Yang, Jia-Cheng Liu *

College of Chemistry and Chemical Engineering, Northwest Normal University, Lanzhou 730070, People's Republic of China

A R T I C L E I N F O

Article history:
Received 25 June 2016
Received in revised form 31 August 2016
Accepted 8 September 2016
Available online 13 September 2016

Keywords:
Metal–organic frameworks
Luminescence sensing
Luminescence quenching
Adsorption

A B S T R A C T

Two metal–organic frameworks (MOFs), $[Ag_2(H_2L)(4,4'\text{-bipy})(\mu_3\text{-OH})]_n$ (**1**) and $[Zn_3(L)_2(bpe)_2(H_2O)_2]_n$ (**2**) were synthesized under hydrothermal conditions using the tricarboxylate and N-containing ligands (H_3L = 3-(3-carboxyphenoxy) phthalic acid, 4,4′-bipy = 4,4′-bipyridine, bpe = 1,2-di(pyridine-4-yl) ethene), and structurally characterized by single-crystal X-ray diffraction analysis, FT-IR spectroscopy, powder X-ray diffraction (PXRD) and thermogravimetric analysis (TGA), furthermore, fluorescent spectra and absorption properties are discussed. Structural analysis reveals that Complex **1** is built from H_3L, 4,4′-bipy and trinucleated Ag to form a three-dimensional (3D) network with a (4,4)-connected topology and a symbol of $(6^3.8^3)_4(8^6)$. As for **2**, a trinucleate secondary building units (SBU), linked by the H_3L ligand generated a one-dimensional (1D) chain, then the two adjacent 1D chains are joined together by bpe ligand, yielding a 1D trapezoidal chain. Our successive application studies indicate that complex **1** shows rapid uptake for methyl orange (MO) and iodine (I_2), compound **2** is an impressive Zn-MOF based sensor for detecting Fe^3+ ions in aqueous solution.

1. Introduction

In recent years, the design and synthesis of Metal–organic frameworks (MOFs) have caught enormous attention of chemical researchers, not only because of their charming architectures and topologies [1], but also for they have shown a variety of potential applications in gas storage and separation [2], catalysis [3], electrochemistry [4], magnetism [5], drug delivery [6], bioimaging [7]and proton conductivity [8]. Generally, coordination polymers could be rationally synthesized by selecting organic ligands and metals. However, the design and composition of crystalline complexes with target topologies as well as multifunction are of great importance topics and are still the tremendously challenges [9,10]. Thus far, a large quantity of MOFs with interesting structures and functional properties have been achieved through optimizing the organic ligands, metal ions/metal clusters, reaction conditions, temperature, pH value, and so on [11,12].

Recently, utilizing MOFs with luminescence property to probe guest species is an increasing trend in the field [13], accompanying many of MOFs based fluorescent probes have been obtained for sensing the transition metal ions [14]. According to reports, the methods to detect metal ions including ion mobility spectroscopy (IMS), inductively coupled plasma (ICP), atomic absorption spectroscopy, voltammetry and X-ray dispersion [15]. Besides, current studies demonstrate that luminescent MOF-based sensors gradually have been enriched due to their unique properties, for instance, facile, sensitive, convenient, fast assays etc. As is well known, trivalent metal ions, especially Fe^{3+}, plays an indispensable role in many biological fields, owe to it broadly existence in the numerous enzymes, and proteins [16]. But only very limited MOFs are synthesized for detecting Fe^{3+} ion until now [17].

In addition, extensive efforts on synthesizing MOFs which have porous structures and are constructed by metal-containing units linked with proper organic groups (carboxylate ligand), have been made for some important applications. For example, efficient adsorption of a variety of chemical pollutants, including toxic metals, organic dyes, iodine, which is of great significance from the viewpoint of the environment [18]. Methyl orange (MO) is the most common organic dyes in wastewater, because of its high chromaticity, strong toxicity, difficulty to degradation and easiness to discompose to carcinogenic aromatic amine under deoxidization condition, azo-dye waste water is considered to be one of the waste water that need to be treated urgently. Traditional methods are usually very complex and not convenient to observe, according to the latest report, photocatalytic degeneration and adsorption are

---

* Corresponding author.
E-mail address: jcliu8@nwnu.edu.cn (J.-C. Liu).

http://dx.doi.org/10.1016/j.ica.2016.09.016
0020-1693/© 2016 Elsevier B.V. All rights reserved.

the effective methods to eliminate pollutants [19]. Removing of MO dye from contaminated water with highly selective and recyclable methods is still have some difficulties. To the best of our knowledge, iodine (I_2) is one of the necessary rare elements for the human body. There are a lot of important functions about iodine deficiency and hypothyroidism, enhancing enzyme activity, promoting absorption of vitamins, disinfecting germs, and so on. But it is very difficult to deal with.

Based on above consideration, in this work, one semi rigid V-shaped multicarboxylate ligands (H_3L) and two auxiliary ligands (4,4′-bipy, bpe, seen in Scheme 1) have been used as molecular building blocks with Ag(I) and Zn(II) ions to get new luminescent MOFs (namely, $[Ag_2(H_2L)(4,4'\text{-bipy})(\mu_3\text{-OH})]_n$ (**1**), $[Zn_3(L)_2(bpe)_2(H_2O)_2]_n$ (**2**)) via solvothermal reaction. Complex **1** presents a 3D multinuclear structure and shows unusual reversible adsorption of I_2 molecules. Complex **2** is a 1D chain, it is developed as a potential material to detect Fe^{3+}. Furthermore, the solid luminescent properties, the phase purity and thermal stability of **1**–**2** are also have been investigated.

2. Experimental

2.1. Materials and physical measurements

All reagents and solvents were purchased and used without further purification. Elemental analyses of C, H and N were performed on a VxRio EL Instrument. FT-IR spectra were recorded in the range 4000–400 cm^{-1} on an FTS 3000 (the United States DIGILAB) spectrometer using KBr pellets. Thermogravimetric analysis (TGA) experiments were carried out on a Perkin-Elmer TG-7 analyzer heated from 25 to 800 °C at a heating rate of 10 °C/min under N_2 atmosphere. Powder X-ray diffraction (PXRD) patterns were obtained on a Philips PW1710–BASED diffractometer at 293 K. The luminescence spectra were carried out on LS-55 (PE USA Inc) fluorescence spectrophotometer at room temperature.

2.2. Syntheses

Syntheses of H_3L. The ligand of 3-(3-carboxyphenoxy)phthalic acid (H_3L) was synthesized in two steps (Scheme S1) [20]:

(a) Synthesis of methyl3-(2,3-dicyanophenoxy)benzoate. A solution of methyl 3-hydroxybenzoate (1.52 g, 10 mmol) in DMF (20 mL) was added anhydrous K_2CO_3 (2.8 g, 20.29 mmol) and the mixture was stirred for 30 min. Then 3-nitrophthalonitrile (1.73 g, 10 mmol) was added, the mixture was continually stirred at 50 °C for 24 h under nitrogen atmosphere. After the reaction mixture was cool down to indoor temperature, K_2CO_3 was filtered off, the filtrate was poured into water of roughly 2 °C (450 mL). After that, a pale yellow solid was gained through a filtration work, which was washed by water and dried in air. Yield: 2.20 g (79.20%).

(b) Synthesis of 3-(3-carboxyphenoxy)phthalic acid (H_3L). The mixture of methyl3- (2,3-dicyanophenoxy)benzoate(2.00 g, 7.2 mmol), ethanol (4 mL), and NaOH (4 mol/L, 54 mL) was refluxed. The mixture was refrigerated to room temperature and undissolved substance was removed by filtration. The pH value of filtrate was adjusted to approximate 4.0 by add HCl (6.0 mol/L) dropwise, a large number of precipitate appear, then static settlement, filtered and laved with distilled water, obtained white solid with a yield of 1.81 g (83%). ESI-MS: *m*/*z* (100%) 302.04 $[M-H]^-$. IR/cm^{-1}(KBr): 3452(w), 1689(s), 1579 (s), 1475(s), 1392(m), 1296(s), 1251(s), 755(s), 983(m) (Fig. S4).

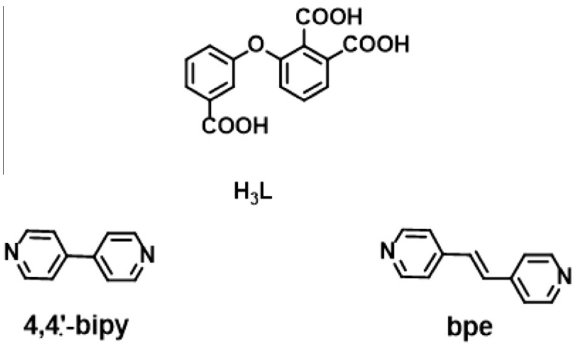

Scheme 1. Schematic structures of H_3L and two N-donor ligands.

2.3. Synthesis of $\{[Ag_2(H_2L)(4,4'\text{-bipy})(\mu_3\text{-OH})]\}_n$ (**1**)

A mixture of $Ag(NO_3)_3{\cdot}6H_2O$ (29.7 mg, 0.10 mmol), H_3L (35.2 mg, 0.20 mmol), 4,4′-bipy (15.6 mg, 0.10 mmol) and H_2O (8 mL) was placed in a parr Teflon-lined stainless steel reactor (25 mL) and heated at 150 °C for 72 h and then slowly cooled to room temperature. Followed by washing with deionized water and drying in air, colorless speculated crystals of **1** were gained (Yield: 71% based on H_3L). Calcd for $Ag_2C_{25}H_{18}N_2O_8$: C, 43.70; H, 2.20; N, 4.08%; found: C, 43.68; H, 2.19; N, 4.06%. IR spectrum (cm^{-1}): 3340(m), 1602(s), 1568(s), 1471(w), 1382(s), 1230(m), 977(w), 806(m) (Fig. S4).

2.4. Synthesis of $\{[Zn_3(L)_2(bpe)_2(H_2O)_2]\}_n$ (**2**)

H_3L (35.2 mg, 0.20 mmol), bpe = 1,2-di(pyridin-4-yl)ethene (28.6 mg, 0.10 mmol) and $Zn(NO_3)_3{\cdot}6H_2O$ (29.7 mg, 0.10 mmol), were commixed in 8 mL H_2O, afterwards, put into a Teflon-lined stainless steel vessel (25 mL), heated to 150 °C for 3 days, and cooled to ambient temperature at 5 °C/h, yellow bulk crystals of **2** with 65% yield (based on H_3L) were acquired. Calcd for $Zn_3C_{54}H_{38}N_4O_{16}$: C, 54.27; H, 3.20; N, 4.69%. Found: C, 54.25; H, 3.09; N, 4.71%. IR (KBr, cm^{-1}): 3328 (m), 1611(s), 1562(s), 1479 (m), 1412(w), 1379(s), 1244(s), 831(m) (Fig. S4).

2.5. Single-crystal X-ray studies

The crystallographic data were measured on a Bruker Smart Apex CCD area detector diffractometer with graphite-monochromated Mo Kα radiation ($\lambda = 0.71073$ Å) for **1**–**2** at 20(2) °C using ω-scan technique, respectively. The diffraction data were employed by the SAINT program, which was also used for the intensity corrections for the Lorentz and polarization effects. Semiempirical absorption corrections were integrated by using SADABS program [21]. The structures were solved by direct methods, and all of the non-hydrogen atoms were refined anisotropically on F^2 by the full-matrix least-squares technique using the SHELXL-97 crystallographic software package. The hydrogen atoms except those of water molecules were generated geometrically and refined isotropically using the riding model. The details of the crystal parameters, data collection and refinements for the compounds are summarized in Table 1. The selected bond lengths (Å) and angles (°) are given in Table S1.

3. Results and discussion

3.1. Crystal structural descriptions

3.1.1. Crystal structure of $\{[Ag_2(H_2L)(4,4'\text{-bipy})(\mu_3\text{-OH})]\}_n$ (**1**)

Compound **1** exhibits a 3D (4,4)-connected net with $(6^3.8^3)_4(8^6)$ topology. It was found that compound **1** crystallizes in the

Table 1
Crystal data and structure refinement for **1** and **2**.

Complexes	1	2
Moiety formula	$C_{25}H_{18}Ag_2N_2O_8$	$C_{54}H_{36}N_4O_{16}Zn_3$
Formula weight	690.15	1192.98
Symmetry space group	*P*2 (1)/c	*P* ī
Temperature:	296 (2) K	296 (2) K
Crystal system	Monoclinic	Triclinic
a (Å)	7.5343 (6)	8.613 (3)
b (Å)	25.243 (2)	14.888 (5)
c (Å)	12.5681 (10)	19.815 (7)
α (deg)	90.00	97.538 (6)
β (deg)	100.3090 (10)	101.190 (5)
γ (deg)	90.00	93.453 (5)
V (Å^3)	2351.7 (3)	2461.6 (14)
Dc (g/cm3)	1.941	1.610
Z	4	2
2θ max (deg)	28.14	25.25
GOF	1.201	0.985
F(0 0 0)	1348.0	1212.0
R$_1$ [I > 2σ(I)][a]	0.0739	0.0491
wR$_2^b$[I > 2σ(I)][b]	0.1776	0.1462

[a] $R_1 = \Sigma||F_o|-|F_c||/\Sigma|F_o|$.
[b] $wR_2 = [\Sigma(|F_o|^2-|F_c|^2)/\Sigma|F_o|^2]^{1/2}$.

Monoclinic P2 (1)/c space group. In the asymmetric unit, two Ag (I) ions, one H_2L^- [22–24] anion of H_3L ligand, one 4,4′-bipy, and one μ_3-OH group were identified. As shown in Fig. 1a, Ag1, Ag2 and Ag3 show parallelly octahedral coordination geometries, while the coordination environments are totally different. Ag1 is surrounded by five O atoms, including four carboxyl oxygen atom (O1, O2, O3B, O7A), one hydroxyl oxygen atom (O8) and one nitrogen atom (N1), to form a distorted octahedral coordination geometry, the Table S1 listed the bond lengths and bond angles around Ag1. Ag2 completed by four oxygen atoms which stem from two carboxyl oxygen atoms adopt monodentate coordination mode (Fig. S3a), another two come from hydroxyl oxygen atoms (O8, O8D) and two nitrogen atoms from two various 4,4′-bipy ligands which occupied the distorted axial positions. Ag3 is located in octahedral geometry with six oxygen atoms from four tricarboxylic acid ligands and two hydroxyl oxygen atoms. Ag2 ion connect the contiguous two Ag1 in a bridging mode to form a trinuclear [(Ag2)(Ag1)$_2$] unit, The trinuclear unit is bridged by the 4,4′-bipy to generate a 1D chain which is Ag1 and Ag2 are linked with 4,4′-bipy in turns. Interestingly, the two Ag ions (Ag2 and Ag3) are held tightly by oxygen atom of μ_3-OH groups to form another 1D zigzag chain (the angle of Ag2-O8-Ag3 is 115.5°) while formed 2D layer (Fig. 1b), Furthermore, the adjoining 2D layers further stack via the H_2L^-, giving a 3D framework along the *a* axis (Fig. 1c). It is worth mentioning that the structure constructed from the H_2L^- and 4,4′-bipy ligands present a porosity by the *a* axis (Fig. S1). Topology analysis exposed that each H_2L^- ligand can be defined as 4-connected nodes, the dinuclear Ag units (Ag1 and Ag3) and Ag2 can be also simplified as 4-connected nodes. Therefore, complex **1** can be classified as a (4,4)-connected net with a Schläfli symbol of $(6^3.8^3)_4(8^6)$ (Fig. 1d).

3.1.2. Crystal structure of {[Zn$_3$(L)$_2$(bpe)$_2$(H$_2$O)$_2$]}$_n$ (**2**)

Compound **2** crystallized in Triclinic space group *P*ī with Z = 2. In the asymmetric unit, contains three Zn(II) atom, two L^{3-} anions, two bpe and two lattices water molecules. As shown in Fig. 2a, Zn1 ion is located in a distorted eight-coordinate octahedral coordination environment, which is defined by three oxygen atoms from three carboxyl groups of H_3L ligands, two oxygen atoms from two coordinated water molecules and a pyridyl nitrogen donors from two bpe ligands. Whereas the Zn2 adopts a seven-coordinated distorted tetrahedron completed with three oxygen atoms from three H_3L ligands and one nitrogen atoms from bpe, homoplastically, Zn3 is a four-coordinated model. According to data of Single-crystal X-ray diffraction analysis, the Zn(II) to O/N distances (Zn-O: 1.940(3)–2.154(3) Å; Zn-N: 2.040(4)-2.107(4) Å) and bond angles are within the normal ranges. The three carboxylated groups from H_3L ligand employed three coordination modes: monodentate, bidentate, chelating monatomic bridging, respectively (Fig. S3b and c). Three Zn (II) atoms can be regard as a trinucleate SBU, the H_3L ligands act as 2-connected node to link Zn3 units into a 1D chain where Zn3 units are supposed to be 4-connected node (Fig. S2). Two adjacent 1D chains are further linked through

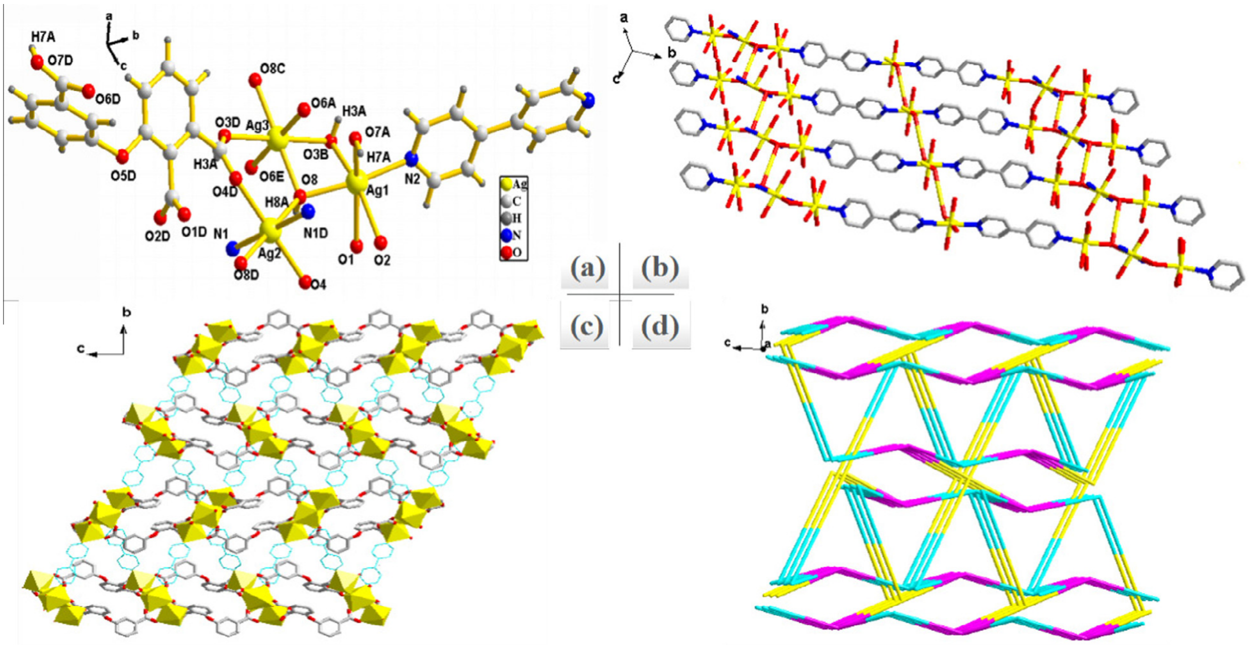

Fig. 1. Structure of compound **1**. (a) Coordination environment of **1**. Symmetry codes: A, −x,−y,−z; B, −x,1−y,−z; C, x,1+y,z; (b) The 2D layers built by Ag atoms and bpe ligand.; (c) The 3D framework of **1**; (d) The (4,4)-connected topology for **1**.

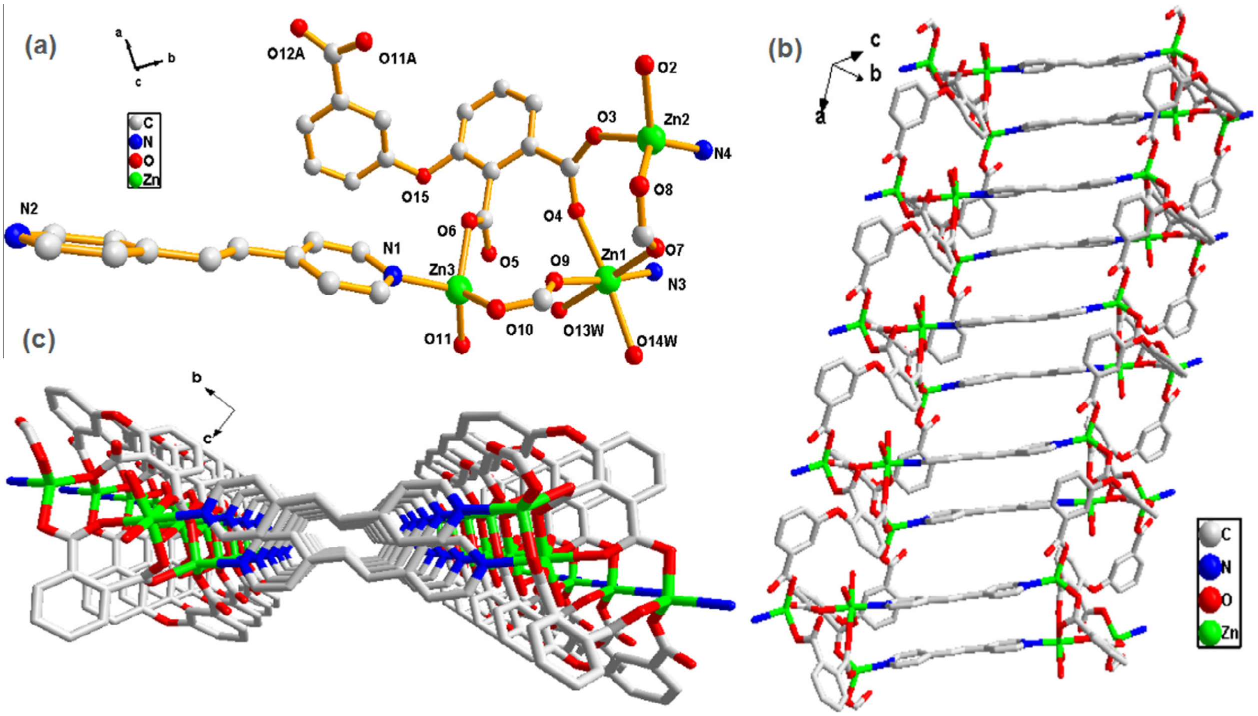

Fig. 2. Structure of compound **2**. (a) Coordination environment of **2**. Hydrogen atoms are omitted for clarity. Symmetry codes: A, 1+x, y, z.; (b) The 1D chain in compound **2** with L^{3-}, bpe and tetra-nuclear Zn cycles connecting each other alternately; (c) This 1D chain is viewed along the given direction.

4,4′-bipyridine, forming a 1D trapezoidal chain (Fig. 2b). Fig. 2c revealed the 1D structure of complex **2** along with *a* axis.

3.2. Phase purity and TGA of the complexes 1–2

We performed PXRD experiments in order to testify the phase purity of complexes 1–2. As illustrated in Fig. S5, the experimental patterns correlate with the simulated patterns, which indicate the crystalline purities of the bulk samples. The preferred orientation of crystals brings about the difference of peaks intensities.

Under an atmosphere of nitrogen, the thermal stabilities of the two complexes have been investigated (Fig. S6). TGA of **1** shows a weight loss of 66.38% around 165–310 °C due to the loss of one μ3-OH group, one bipy molecules and a H_3L ligand (calc. wt% 66.27) and then the network happened to collapse. As for complex **2**, the first weight loss of 3.12% was observed in the temperature about 96 °C, corresponding to loss of two coordinated water molecules, and the dehydrated sample, $[Zn_3(L)_2(bpe)_2]_n$ is stable up to 270 °C. The second major weight loss of 80.49% around 270–507 °C which can be assigned due to the loss of two L ligands and two bpe spacers (calc. wt% 80.56), after which it begins to decompose.

3.3. Selective adsorption of organic dyes and I_2

For complex **1** possess a 3D construction with tiny holes, we decided to study the adsorption ability of compound **1** for organic dyes. In the experiments, aqueous solution of methylene blue (MB), methyl orange (MO) and rhodamine B (RhB) as model organic pollutants were carried out. 2 mg of crystals **1** were respectively dipped into aqueous solutions of MO, MB and RhB (20 ppm, 4 mL) at ambient temperature, then agitate for 10 min under dark environment. Found that the color of MB and RhB barely changed, on the contrary, the orange of MO solution faded away slowly to colorless (Fig. S7). Tested by UV, the concentration of MB/RhB in water decreased slightly (from the initial 20 ppm to final 19.64 ppm or19.12 ppm), during the same process, while the MO concentration almost decreasing to 4.85 ppm (Fig. 3). Therefore, the adsorptive capacity of **1** for MB/RhB is negligible, it can effectively remove MO from aqueous solution.

To preferably research the adsorptive capacity of complex **1**, 20 mg of compound was put in 0.02 mmol/L aqueous solution of MO 50 mL and magnetically stirred under dark condition, then every a period of time, taking out 3.0 mL samples for analysis by UV–vis spectroscopy. As figure placed as Fig. 4a, the absorption peaks intensity of MO were decrease along with time increasingly, vary 0–65 min. After 65 min, the intensity not changed anymore, the initial losses ratio of MO reaches 93% for **1**. Moreover, the stability of the framework has been confirmed by the comparative the X-ray powder diffraction patterns of **1**, before and after immersing in the solution of MO for 24 h (Fig. S5).

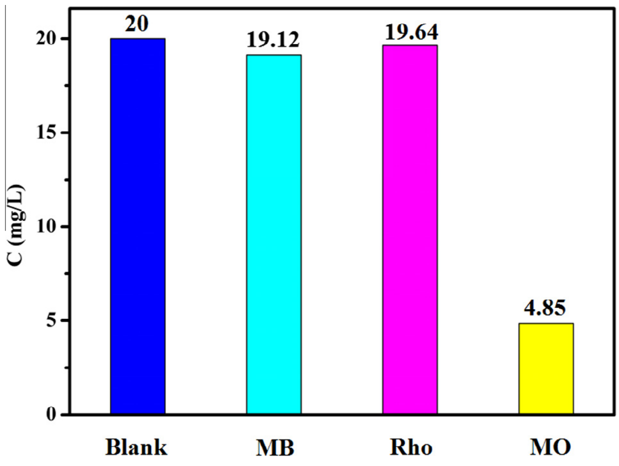

Fig. 3. Concentration of MO, MB and Rhodamine B by addition **1** (2 mg) in 3 mL of dye-containing aqueous solutions.

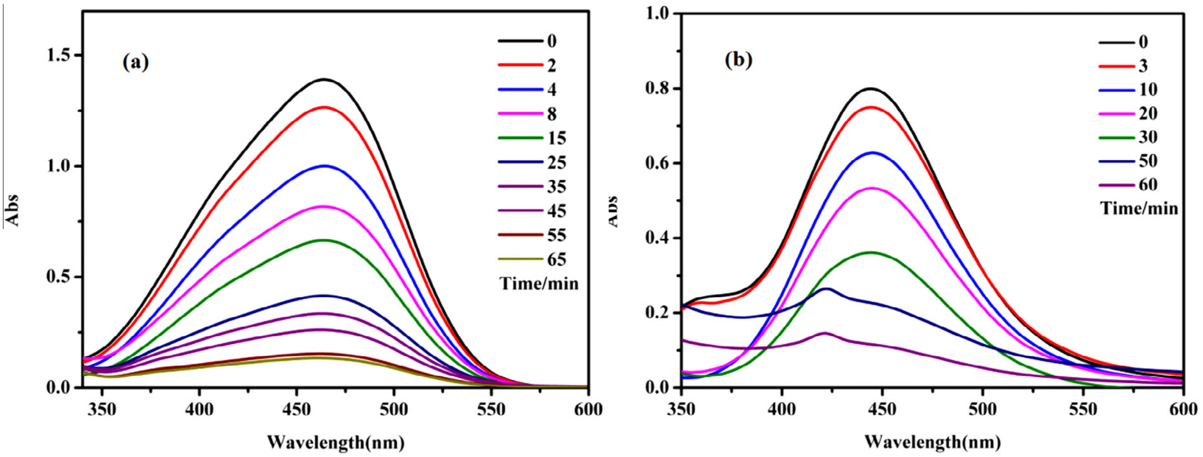

Fig. 4. Theultraviolet–visible light (UV–vis) absorption spectra of compound **1** for Methyl orange (MO) and I_2 (b) in aqueous solution.

Meanwhile, the potential uptaking applications of **1** in separating I_2 were also examined. Crystal **1** was selected to soak in the ethanol solution of I_2 (0.1 mM), which showed the yellow solutions of I_2 fade slowly to light yellow until colorless with time (Fig. S7). Following Fig. 4b, the intensity of absorption bands became weaker with time (means concentration of I_2 molecules were continue to reduce). The phenomenon of adsorption due to the small porosity in the 3D construction, both I_2 and MO are small moleculars than MB/RhO, complex **1** can storage these substances in the hole, in the other words, this is the explanation of why MB/RhO can't be bleed [25].

3.4. Luminescence properties

Metal-organic coordination polymers, particularly those including d^{10} ions have been investigated for their photo luminescent properties and potential applications for wide applications in the fluorescence emitting materials [26]. Not only for their multiple surroundings but also for their variable luminescent characters, for instance, interaction with functional ligands, connection, or adopting different coordination modes, guest encapsulation or release, and the temperature variation. Therefore, as depicted in Fig. S8a, the solid-state fluorescent properties of H_3L ligand and compounds **1**, 2 have been explored at room temperature. The maximum emission band are observed at 424 nm (λ_{ex} = 280 nm) for compound **1**, 471 nm (λ_{ex} = 350 nm) for compound **2**, respectively. And the free ligand H_3L display emission band at 343 nm upon excitation at 280 nm, possibly, arising from the intraligand $\pi-\pi*$ transitions of the aromatic rings. In comparison with the free H_3L, the maximum emissions of **1** and 2 are distinctly red-shifted, which may be attributed to the mixture effects of intraligand charge transfer and ligand-to-metal charge transfer (LMCT) [27]. Moreover, complex **2** has an enhanced luminescence intensity compared to **1**, which can be explained by the differences in the structures and metal. More importantly, because of the visible emission of **2** under ultraviolet light, it's sensing properties were further studied to probe different metal ions in aqueous solution.

3.5. Luminescence sensing functions of Fe^{3+} of compound **2**

At present, some coordination polymers are usually used as highly selective luminescent probes to metal ions. In consideration of the condition of metal ions recognition, we also measured the fluorescence emission of the suspension (Fig. S8b). Based on experimental research, the suspension presents luminescence characteristic strong resemblance of **2** in the solid state, which means complex **2** has a comparative good water stability, however, the luminescent value of H_3L ligands changed extremely, and complex **1** has weak photoluminescence (PL) intensity. Hence, in this work, we select compounds **2** to explore the potential sensing functions

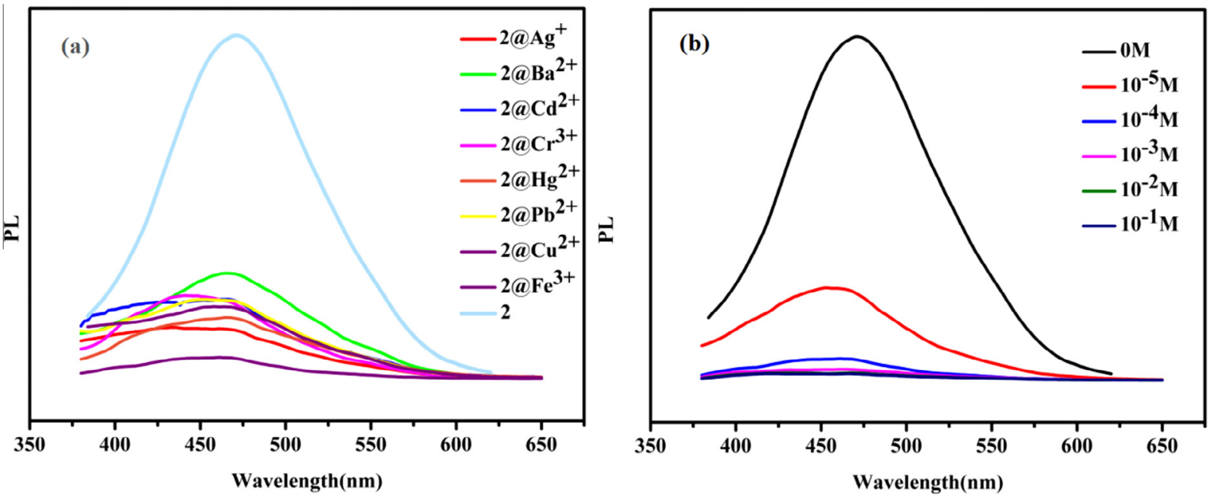

Fig. 5. (a) Luminescence spectra of **2**@M^{n+} suspensions; (b)Luminescence spectra of complex **2** immersed to Fe^{3+} aqueous solutions with different concentrations.

of metal ions. The method as follows, As-synthesized **2** (5 mg) was immersed in 3 mL distilled water with 1.0×10^{-3} mol·L^{-1} M$(NO_3)_n$ (M = Cr^{3+}, Fe^{3+}, Cu^{2+}, Ag^+, Cd^{2+}, Ba^{2+}, Hg^{2+} and Pb^{2+}) for 1 h to form the suspension of **2**@M^{n+} for sensing studies. The luminescent properties of the suspension were recorded in Fig. 5a. The results revealed that the luminescence intensities were changed on the addition of various metal ions compared to the blank sample. Although with adding Cr^{3+}, Fe^{3+}, Cu^{2+}, Ag^+, Cd^{2+}, Ba^{2+}, Hg^{2+} and Pb^{2+}, there is inordinately quenching behavior in suspension, however, comparing with Fe^{3+}, the decreasing degree is not obvious. Thus, compound **2** can be identified as a candidate for selective luminescence sensing to Fe^{3+} ions. Besides, in order to get a detail understanding of this phenomenon, the luminescence intensities of **2**@Fe^{3+} suspension by varying concentration of Fe^{3+} ions in the range of 10^{-5}–10^{-1} M was explored (Fig. 5b). As a result, accompanied by the increase of Fe^{3+}, the luminescence intensities of **2** decreases gradually, and luminescence quenched don't changed until the concentration of Fe^{3+} up to 10^{-3} M.

The probable mechanism of the quenching effect of **2** suspension caused by Fe^{3+} can be considered as an electron transfer between the donor (the organic ligands) and the acceptor (the metal ions). the residual oxygen atoms of the carboxylates which come from the L^{3-} ligands can treat as electrons donors. The electrons are shifted from the donor to the acceptor upon ultraviolet light excitation, leading to luminescence quenching [28–29]. In other words, it is notable that excitation spectrum of compound **2** centered at 350 nm which is apparently overlapped by the absorption band of Fe^{3+} (the Fe^{3+} assumes a broad absorption band from 200 to 390 nm) [30–31]. Therefore, the photoluminescence quenching function could be due to the energy transfers from the organic ligand to Fe^{3+} upon excitation.

4. Conclusion

In summary, we employed a semi-rigid carboxylate ligand (3-(3-carboxyphenoxy) phthalic acid), different N-donor auxiliary ligands to gain two MOFs, namely, $[Ag_2(H_2L)(4,4'\text{-bipy})(\mu_3\text{-OH})]_n$ (**1**) and $[Zn_3(L)_2(bpe)_2(H_2O)_2]_n$ (**2**) which exhibit structural diversity. Furthermore, we explored the uptake ability of methyl orange (MO) and iodine (I_2) in **1**, and complex **2** exhibits the fluorescence sense of Fe^{3+} ions in aqueous solution.

Acknowledgements

This work was supported by grants from the Natural Science Foundation of China (Nos. 21461023 and 21361023) and Gansu Provincial Natural Science Foundation of China (No. 1606RJZA110).

Appendix A. Supplementary data

CCDC 1462880 (1) and 1462881 (2) contain the supplementary crystallographic data for three complexes. These data can be obtained free of charge via http://www.ccdc.cam.ac. uk/conts/retrieving.html, or from the Cambridge Crystallographic Data Centre, 12 Union Road, Cambridge CB2 1EZ, UK; fax: (+44) 1223 336 033.

Supplementary data associated with this article can be found, in the online version, at http://dx.doi.org/10.1016/j.ica.2016.09.016.

References

[1] Y.L. Gai, F.L. Jiang, K.C. Xiong, L. Chen, D.Q. Yuan, L.J. Zhang, K. Zhou, M.C. Hong, Cryst. Growth Des. 12 (2012) 2079.

[2] C.S. Hawes, G.P. Knowles, A.L. Chaffee, D.R. Turner, S.R. Batten, Cryst. Growth Des. 15 (2015) 3417.

[3] H.Y. Ren, R.X. Yao, X.M. Zhang, Inorg. Chem. 54 (2015) 6312.

[4] M.G. Cowan, J. Olguín, S. Narayanaswamy, J.L. Tallon, S. Brooker, J. Am. Chem. Soc. 134 (2012) 2892.

[5] P. Mahata, S. Natarajan, P. Panissod, M. Drillon, J. Am. Chem. Soc. 131 (2009) 10140.

[6] S.Y. Zhang, W. Shi, P. Cheng, M.J. Zaworotko, J. Am. Chem. Soc. 137 (2015) 12203.

[7] D. Liu, K. Lu, C. Poon, W. Lin, Inorg. Chem. 53 (2014) 1916.

[8] I. Mihalcea, C. Volkringer, N. Henry, T. Loiseau, Inorg. Chem. 51 (2012) 9610.

[9] S. Ma, D. Sun, M. Ambrogio, J.A. Fillinger, S. Parkin, H.C. Zhou, J. Am. Chem. Soc. 129 (2007) 1858.

[10] H. Wang, F.Y. Yi, S. Dang, W.G. Tian, Z.M. Sun, Cryst. Growth Des. 14 (2013) 147.

[11] S.Q. Zhang, F.L. Jiang, M.Y. Wu, J. Ma, Y. Bu, M.C. Hong, Cryst. Growth Des. 12 (2012) 1452.

[12] C.K. Brozek, M. Dinca, J. Am. Chem. Soc. 135 (2013).

[13] A.X. Zhu, Z.Z. Qiu, L.B. Yang, X.D. Fang, S.J. Chen, Q.Q. Xu, Q.X. Li, CrystEngComm 17 (2015) 4787.

[14] S.Y. Moon, N.R. Cha, Y.H. Kim, S.K. Chang, J. Org. Chem. 69 (2004) 181.

[15] A.X. Tian, Y.L. Ning, Y. Yang, X. Hou, J. Ying, G.C. Liu, J.W. Zhang, X.L. Wang, Dalton Trans. 44 (2015) 16486.

[16] Q. Zhao, F.Y. Li, C.H. Huang, Chem. Soc. Rev. 39 (2010) 3007.

[17] Y.L. Wu, G.P. Yang, X. Zhou, J. Li, Y. Ning, Y.Y. Wang, Dalton Trans. 44 (2015) 10385.

[18] C. Zou, Z.J. Zhang, X. Xu, Q.H. Gong, J. Li, C.D. Wu, J. Am. Chem. Soc. 134 (2012) 87.

[19] (a) Y. Hu, F. Luo, F.F. Dong, Chem. Commun. 47 (2011) 761;
(b) Y.Q. Chen, S.J. Liu, Y.W. Li, G.R. Li, K.H. He, Y.K. Qu, T.L. Hu, X.H. Bu, Cryst. Growth Des. 12 (2012) 5426;
(c) H.J. Pang, H.Y. Ma, J. Peng, C.J. Zhang, P.P. Zhang, Z.M. Su, CrystEngComm 13 (2011) 7079.

[20] C.D. Si, D.C. Hu, Y. Fan, Y. Wu, X.Q. Yao, Y.X. Yang, J.C. Liu, Cryst. Growth Des. 15 (2015) 2419.

[21] (a) SAINT, Program for Data Extraction and Reduction, Bruker AXS, Inc., Madison, WI, 2001;
(b) G.M. Sheldrick, SADABS; University of Göttingen: Göttingen, Germany, 1997.

[22] C.N. Banti, A.D. Giannoulis, N. Kourkoumelis, A.M. Owczarzak, M. Kubicki, S.K. Hadjikakou, J. Inorg. Biochem. 142 (2015) 132.

[23] H.M. Titi, I. Goldberg, CrystEngComm 12 (2010) 3914.

[24] J. Hunger, H. Krautscheid, J. Sieler, Cryst. Growth Des. 9 (2009) 4613.

[25] L.L. Lv, J. Yang, H.M. Zhang, Y.Y. Liu, J.F. Ma, Inorg. Chem. 54 (2015) 1744.

[26] (a) L. Luo, K. Chen, Q. Liu, Y. Lu, T.A. Okamura, G.C. Lv, Y. Zhao, W.Y. Sun, Cryst. Growth Des. 13 (2013) 2312;
(b) A. Santra, P.K. Bharadwaj, Cryst. Growth Des. 14 (2014) 1476.

[27] S.L. Zheng, J.H. Yang, X.L. Yu, X.M. Chen, W.T. Wong, Inorg. Chem. 43 (2004) 830.

[28] Z.M. Hao, G.C. Yang, X.Z. Song, M. Zhu, X. Meng, S.N. Zhao, S.Y. Song, H.J. Zhang, J. Mater. Chem. A. 2 (2014) 237.

[29] X. Meng, X.Z. Song, S.Y. Song, G.C. Yang, M. Zhu, Z.M. Hao, S.N. Zhao, H.J. Zhang, Chem. Commun. 49 (2013) 8483.

[30] Y.T. Liang, G.P. Yang, B. Liu, Y.T. Yan, Zh.P. Xi, Y.Y. Wang, Dalton Trans. 44 (2015) 13325.

[31] H. Xu, F. Liu, Y. Cui, B. Chen, G. Qian, Chem. Commun. 47 (2011) 3153.